A High-Order CUF–FEM Framework for Thermo-Piezo-Mechanically Actuated Composite Structures

Bracaglia F. *, Pagani A. †, Zappino E. ‡, Carrera E. §
Politecnico di Torino, Corso Duca degli Abruzzi, 24, Torino, Italy, 10129

F. Moleiro¶ and A.L. Araújo ‖
Instituto Superior Técnico, Universidade de Lisboa, Avenida Rovisco Pais, Lisboa, Portugal, 11049-001

The present work investigates the geometrically nonlinear thermo-piezo-elastic response of composite plates with piezoelectric layers. The electric field allows control of the critical buckling temperature and the post-buckling deflection. The governing equations are derived from the Principle of Virtual Displacement (PVD) with the full Green-Lagrange strain tensor. A decoupled approach is considered to describe the multiphysics problem. The nonlinear problem is solved using the Newton-Raphson method with an arc-length constraint. The through-thickness stress distributions are also investigated, focusing on the interface between the composite laminate and the piezoelectric layers.

I. Introduction

Thin-walled composite structures are widely employed in aerospace applications to reduce weight while maintaining stiffness and strength. To improve the performance of these structures under specific loading conditions, so-called smart structures have been introduced and widely studied in recent years. Among the large field of smart structures, a significant group consists of panels with piezoelectric actuators that, when activated, can apply a chosen force to the structure. The interest in these structures is driven by their ability to adapt their response to changing operational conditions. Furthermore, this type of adaptation differs from other approaches because the actuating mechanism is integrated in the structure itself and is activated by an applied electric field.

Among the numerous advantages, there is the possibility to activate the piezoelectric patch to enable various engineering applications such as active shape control, noise reduction, vibration control, and retarding or avoiding buckling. The piezoelectric layer is usually a few millimeters thick, with research moving towards a few microns as dimensions get smaller, induced electro-thermo-mechanical fields grow larger, and activation becomes more efficient [1]. However, due to the flexibility of these structures and the combination of different materials (piezoelectric and structural materials), it is necessary to conduct geometrically nonlinear analyses to describe the structural response under certain loads. In this manner, the description is not restricted to small displacements and rotations, allowing investigation of buckling and post-buckling configurations.

hinneBuckling is a non-linear phenomenon that occurs under compressive loading and results in a sudden change in the shape of thin structures. The displacement in the post-buckling configuration is typically very pronounced and can occur smoothly without causing permanent damage or can occur abruptly with catastrophic outcomes. When buckling starts, failure does not necessarily happen [2]. In fact, some structures can be designed to carry the applied load even in buckled configurations, whereas others must avoid it. A compressive stress state can be caused by an applied mechanical load and is readily increased by elevated temperature acting on the structure [3]. The thermal load acts on aerospace structures, such as orbit components and supersonic and hypersonic vehicles, due to solar radiation or aerodynamic drag [4, 5].

Various studies have examined the piezoelectric patch's response to phenomena such as flutter and vibration control [6], demonstrating that these phenomena can be retarded or modified by activating these materials. In this field, the piezoelectric patches can be applied on the plate to avoid or retard thermal buckling or to control the post-buckling

*Ph.D. Student, Department of Mechanical and Aerospace Engineering; francesca.bracaglia@polito.it.
†Full Professor, Department of Mechanical and Aerospace Engineering; alfonso.pagani@polito.it
‡Associate Professor, Department of Mechanical and Aerospace Engineering; enrico.zappino@polito.it
§Full Professor, Department of Mechanical and Aerospace Engineering; erasmo.carrera@polito.it
¶Associate Professor, Department of Mechanical Engineering; filipa.moleiro@tecnico.ulisboa.pt.
‖Associate Professor, Department of Mechanical Engineering; aurelio.araujo@tecnico.ulisboa.pt

configuration. Linearized buckling analysis is conducted with different approaches [7–9], where the influence of lamination, position of the piezoelectric patches, and boundary conditions is investigated. Then, nonlinear analyses have been proposed [10, 11] to evaluate the impact of activation on the postbuckling displacement.

It is clear that variations in temperature acting on a structure result in different thermal strains, depending on the material's properties. Piezoelectric patches are applied to composite and isotropic materials for control purposes, but typically, the thermal expansion coefficients of these materials differ. This strain mismatch between the patch and the structure can lead to high interlaminar stresses between the two materials [12]. For this reason, an accurate description of the interlaminar stresses is necessary.

The present work focuses on evaluating the effect of applying a piezoelectric patch on the geometrically nonlinear response of plates under thermal loading. The effect of the piezoelectric actuation is investigated to act on the thermal-buckling and post-buckling configuration, focusing on 1) the effect of the position of the piezo patch on retarding buckling and modifying post-buckling shape, and 2) the description of of the heightened piezo-thermo-mechanical stresses at the interface of the different materials.

II. Preliminary concepts

The problem is described using a decoupled multiphysics approach. The only unknowns of the problem are the displacements in the three directions, and thermal and piezoelectric contributions are considered as equivalent loads applied to the structure. With this approach, the problem is easily described with a reduction in degrees of freedom compared to a fully coupled approach, without losing accuracy. The displacement vector is given by Eq. (1):

$$\boldsymbol{u}^T(x, y, z) = \left(u_x, u_y, u_z\right) \tag{1}$$

The displacement vector can be written employing Carrera Unified Formulation (CUF), which allows the expression of the unknowns of the problem through a combination of expansion functions and *generalized* 2D displacements, as reported in Eq. (2). In this way, the use of different kinematic theories can be implemented straightforwardly without any change in the formalism of the problem or in the governing equations.

$$\boldsymbol{u}(x, y, z) = F_\tau(z)\boldsymbol{u}_\tau(x, y) \quad \tau = 1, 2, ..., N \tag{2}$$

In the equation, $F_\tau(z)$ represents the expansion function, $\boldsymbol{u}_\tau(x, y)$ denotes the *generalized* 2D displacements, N is the number of terms employed in the expansion, and the double subscript means summation. Using the expansion functions, it is possible to express different kinematic theories employing different classes of functions. The most commonly used classes are Taylor Expansion (TE) functions, which are hierarchical polynomials whose order matches the order of expansion. The second class consists of Lagrange Expansion (LE) functions, which provide an explicit through-the-thickness description based on physical nodes. CUF is employed in conjunction with the FEM as expressed by Eq. (3):

$$\boldsymbol{u}(x, y, z) = F_\tau(z)N_i(x, y)\boldsymbol{q}_{\tau i} \quad i = 1, 2, ..., M \tag{3}$$

$N_i(x, y)$ denotes the shape function that describes the in-plane finite elements, which are Q9 in this work, and $\boldsymbol{q}_{\tau i}$ represents the nodal displacement vector, being $\boldsymbol{q}^T_{\tau i} = \left(q_{x_{\tau i}},\ q_{y_{\tau i}},\ q_{z_{\tau i}}\right)$. In this study, M is the number of nodes adopted in the finite element. Naturally the thickness functions and the shape functions are independent of each other, therefore, M and N can be selected independently and arbitrarily.

The geometrical relations link the mechanical strains $\boldsymbol{\varepsilon}_m$ to the displacement field $\boldsymbol{u}$ and are expressed through the differential operator reported in Eq. (4), where the relation expresses the full Green-Lagrange strain tensor.

$$\boldsymbol{\varepsilon}_m = \boldsymbol{\varepsilon}_l + \boldsymbol{\varepsilon}_{nl} = (\boldsymbol{b}_l + \boldsymbol{b}_{nl})\,\boldsymbol{u} \tag{4}$$

In this equation, the geometric differential operator $\boldsymbol{b}$ is divided into its linear and nonlinear components, whose explicit formulation is well described in the literature. The subscript l and nl refer to the linear and the nonlinear parts, respectively.

The constitutive relationship between stress and strain is expressed through the elastic coefficient matrix $\boldsymbol{C}$ in Eq. (5). The explicit formulation of the matrix is well known; hereafter, it is employed as defined in the Cartesian global reference system, and the explicit formulation can be found in the literature [13].

$$\boldsymbol{\sigma} = \boldsymbol{C}\boldsymbol{\varepsilon} \tag{5}$$

Due to the decoupled approach, the stresses and strains can be split into mechanical, thermal, and piezoelectric components as expressed by Eqs. (6) and (7). Mechanical strains are expressed in terms of a geometrical relation; on the other hand, thermal and piezoelectric components are obtained using the definitions of thermal expansion and piezoelectric strain. The material thermal expansion vector is $\boldsymbol{\alpha}^T = (\alpha_1, \alpha_2, \alpha_3, 0, 0, 0)$ and the piezoelectric strain coefficient is $\boldsymbol{d}$ which is a matrix 6×3 with the only non-null coefficients being d_{31} and d_{32}.

$$\boldsymbol{\varepsilon} = \boldsymbol{\varepsilon}_m + \boldsymbol{\varepsilon}_\theta + \boldsymbol{\varepsilon}_p = \boldsymbol{\varepsilon}_m - \boldsymbol{\alpha}\Delta\mathcal{T} - \boldsymbol{d}\mathcal{E} = \boldsymbol{\varepsilon}_l + \boldsymbol{\varepsilon}_{nl} - \boldsymbol{\alpha}\Delta\mathcal{T} - \boldsymbol{d}\mathcal{E} \tag{6}$$

$$\boldsymbol{\sigma} = \boldsymbol{C}\boldsymbol{\varepsilon} = \boldsymbol{C}\left(\boldsymbol{\varepsilon}_m + \boldsymbol{\varepsilon}_\theta + \boldsymbol{\varepsilon}_p\right) = \boldsymbol{C}\left(\boldsymbol{\varepsilon}_m - \boldsymbol{\alpha}\Delta\mathcal{T} - \boldsymbol{d}\mathcal{E}\right) = \boldsymbol{\sigma}_m - \boldsymbol{\beta}\Delta\mathcal{T} - \boldsymbol{e}\mathcal{E} = \boldsymbol{\sigma}_l + \boldsymbol{\sigma}_{nl} + \boldsymbol{\sigma}_\theta + \boldsymbol{\sigma}_p \tag{7}$$

The combination of the elastic coefficient matrix $\boldsymbol{C}$ along with $\boldsymbol{\alpha}$ and $\boldsymbol{d}$ results in the vector $\boldsymbol{\beta}$ and matrix $\boldsymbol{e}$, respectively. In Eqs. (6) and (7), $\Delta\mathcal{T}$ is the applied over-temperature, assumed to be uniform throughout the plate, and $\mathcal{E}$ is the electric field.

III. Geometrically nonlinear thermo-piezo-mechanical equations

A. Governing equation

The equality between the virtual work of the internal forces δL_{int} and the virtual work of the external load δL_{ext} is expressed by Eq. (8) [14].

$$\delta L_{int} = \delta L_{ext} \tag{8}$$

The virtual external load is null considering there is no mechanical force applied, and only the virtual internal work arises, collecting the thermal and piezoelectric effects, as follows in Eq. (9):

$$\delta L_{int} = \int_V \delta\boldsymbol{\varepsilon}^T \boldsymbol{\sigma} dV = 0 \tag{9}$$

where it is possible to substitute the prior relations given by Eqs. (6) and (7) for strain and stress, respectively:

$$\begin{aligned} \delta L_{int} &= \int_V \delta\boldsymbol{\varepsilon}^T \boldsymbol{\sigma} dV = \int_V \delta\left(\boldsymbol{\varepsilon}_m + \boldsymbol{\varepsilon}_\theta + \boldsymbol{\varepsilon}_p\right)^T \boldsymbol{C}\left(\boldsymbol{\varepsilon}_m + \boldsymbol{\varepsilon}_\theta + \boldsymbol{\varepsilon}_p\right) dV \\ &= \int_V \delta\boldsymbol{\varepsilon}_m^T \boldsymbol{C}\boldsymbol{\varepsilon}_m dV + \int_V \delta\boldsymbol{\varepsilon}_m^T \boldsymbol{C}\boldsymbol{\varepsilon}_\theta dV + \int_V \delta\boldsymbol{\varepsilon}_m^T \boldsymbol{C}\boldsymbol{\varepsilon}_p dV \end{aligned} \tag{10}$$

Since the virtual variations $\delta\boldsymbol{\varepsilon}_p$ and $\delta\boldsymbol{\varepsilon}_\theta$ are null, and substituting Eq. (7), the virtual work of the internal forces becomes as follows:

$$\delta L_{int} = \int_V \delta\boldsymbol{\varepsilon}_m^T \boldsymbol{C}\boldsymbol{\varepsilon}_m dV - \int_V \delta\boldsymbol{\varepsilon}_m^T \boldsymbol{\beta}\Delta\mathcal{T} dV - \int_V \delta\boldsymbol{\varepsilon}_m^T \boldsymbol{e}\mathcal{E} dV \tag{11}$$

From Eq. (11), it is possible to define the secant stiffness matrix, the thermal and the piezoelectric load vectors. The first term of Eq. (11) depends only on the mechanical strain components and defines the purely mechanical secant stiffness matrix, as given by Eq. (12):

$$\begin{aligned} \int_V \delta\boldsymbol{\varepsilon}_m^T \boldsymbol{C}\boldsymbol{\varepsilon}_m dV &= \int_V \delta\left(\boldsymbol{\varepsilon}_l + \boldsymbol{\varepsilon}_{nl}\right)^T \boldsymbol{C}\left(\boldsymbol{\varepsilon}_l + \boldsymbol{\varepsilon}_{nl}\right) dV \\ &= \int_V \delta\boldsymbol{\varepsilon}_l^T \boldsymbol{C}\boldsymbol{\varepsilon}_l dV + \int_V \delta\boldsymbol{\varepsilon}_l^T \boldsymbol{C}\boldsymbol{\varepsilon}_{nl} dV + \int_V \delta\boldsymbol{\varepsilon}_{nl}^T \boldsymbol{C}\boldsymbol{\varepsilon}_l dV + \int_V \delta\boldsymbol{\varepsilon}_{nl}^T \boldsymbol{C}\boldsymbol{\varepsilon}_{nl} dV \\ &= \delta\boldsymbol{q}_{sj}^T \left[\boldsymbol{K}_0^{ij\tau s} + \boldsymbol{K}_{lnl}^{ij\tau s} + \boldsymbol{K}_{nll}^{ij\tau s} + \boldsymbol{K}_{nlnl}^{ij\tau s}\right] \boldsymbol{q}_{\tau i} \end{aligned} \tag{12}$$

The explicit formulation of these matrices can be found in [15]. Substituting CUF and FEM into equation (11), the stiffness matrix components can be written in indicial notation in terms of the indices $ij\tau s$ which represents the description of the Fundamental Nuclei (FNs) of the matrices. These FNs are the simplest components of matrices and vectors written for the displacement vector, being 3×3 matrices and 3×1 vectors. The complete matrices or vectors can then be obtained through an assembly procedure build from loops over the nodes and elements. The complete description can be found in [16].

From the second term of Eq. (11) the thermal load vector is obtained as given below:

$$\begin{aligned}\int_V \delta\boldsymbol{\varepsilon}_m^T \boldsymbol{\beta}\Delta\mathcal{T} dV = \int_V \delta\left(\boldsymbol{\varepsilon}_l^T + \boldsymbol{\varepsilon}_{nl}^T\right)\boldsymbol{\beta}\Delta\mathcal{T} dV = \int_V \delta\boldsymbol{\varepsilon}_l^T \boldsymbol{\beta}\Delta\mathcal{T} dV + \int_V \delta\boldsymbol{\varepsilon}_{nl}^T \boldsymbol{\beta}\Delta\mathcal{T} dV \\ = \int_V \delta\left(\boldsymbol{b}_l F_s(z) N_j(x,y)\boldsymbol{q}_{sj}\right)^T \boldsymbol{\beta}\Delta\mathcal{T} dV + \int_V \delta\left(\boldsymbol{b}_{nl} F_s(z) N_j(x,y)\boldsymbol{q}_{sj}\right)^T \boldsymbol{\beta}\Delta\mathcal{T} dV\end{aligned} \tag{13}$$

where the application of the differential matrices $\boldsymbol{b}_l$ and $\boldsymbol{b}_{nl}$ on the shape and expansion functions results in the matrices $\boldsymbol{B}_l^{sj}$ and $\boldsymbol{B}_{nl}^{sj}$. It is possible to demonstrate that $\delta(\boldsymbol{B}_l^{sj}\boldsymbol{q}_{sj}) = \boldsymbol{B}_l^{sj}\delta\boldsymbol{q}_{sj}$ and $\delta(\boldsymbol{B}_{nl}^{sj}\boldsymbol{q}_{sj}) = 2\boldsymbol{B}_{nl}^{sj}\delta\boldsymbol{q}_{sj}$. Hence, substituting the definition of these matrices into Eq. (13), leads to Eq. (14).

$$\begin{aligned}\int_V \delta\boldsymbol{q}_{sj}^T \boldsymbol{B}_l^{sjT}\boldsymbol{\beta}\Delta\mathcal{T} dV + 2\int_V \delta\boldsymbol{q}_{sj}^T \boldsymbol{B}_{nl}^{sjT}\boldsymbol{\beta}\Delta\mathcal{T} dV =& \delta\boldsymbol{q}_{sj}^T\left[\int_V \boldsymbol{B}_l^{sjT}\boldsymbol{\beta}\Delta\mathcal{T} dV + \int_V 2\boldsymbol{B}_{nl}^{sjT}\boldsymbol{\beta}\Delta\mathcal{T} dV\right] \\ =& \delta\boldsymbol{q}_{sj}^T\left[\boldsymbol{F}_{\theta_l}^{sj} + \boldsymbol{F}_{\theta_{nl}}^{sj}\right]\end{aligned} \tag{14}$$

The explicit formulation of this vector can be found in [15]. Following the same procedure, starting from the last term of Eq. (11) the piezoelectric load vector describing the activation of the patches is obtained as given by Eq. (15)

$$\begin{aligned}\int_V \delta\boldsymbol{\varepsilon}_m^T \boldsymbol{e}\mathcal{E} dV = \int_V \delta\left(\boldsymbol{\varepsilon}_l^T + \boldsymbol{\varepsilon}_{nl}^T\right)\boldsymbol{e}\mathcal{E} dV = \int_V \delta\boldsymbol{\varepsilon}_l^T \boldsymbol{e}\mathcal{E} dV + \int_V \delta\boldsymbol{\varepsilon}_{nl}^T \boldsymbol{e}\mathcal{E} dV \\ = \int_V \delta\boldsymbol{q}_{sj}^T \boldsymbol{B}_l^{sjT}\boldsymbol{e}\mathcal{E} dV + 2\int_V \delta\boldsymbol{q}_{sj}^T \boldsymbol{B}_{nl}^{sjT}\boldsymbol{e}\mathcal{E} dV \\ = \delta\boldsymbol{q}_{sj}^T\left[\int_V \boldsymbol{B}_l^{sjT}\boldsymbol{e}\mathcal{E} dV + \int_V 2\boldsymbol{B}_{nl}^{sjT}\boldsymbol{e}\mathcal{E} dV\right] = \delta\boldsymbol{q}_{sj}^T\left[\boldsymbol{F}_{p_l}^{sj} + \boldsymbol{F}_{p_{nl}}^{sj}\right]\end{aligned} \tag{15}$$

The explicit formulation of the piezoelectric load is expressed by Eq. (16), where the linear and nonlinear parts are represented by two vectors.

$$\boldsymbol{F}_{p_l}^{sj} = \begin{Bmatrix}\mathcal{E}\int_V e_{(3,1)} F_s N_{j,x} dV \\ \mathcal{E}\int_V e_{(3,2)} F_s N_{j,y} dV \\ \mathcal{E}\int_V e_{(3,3)} F_{s,z} N_j dV\end{Bmatrix} \boldsymbol{F}_{p_{nl}}^{sj} = \begin{Bmatrix}\mathcal{E}\int_V \left(e_{(3,1)} u_{x,x} F_s N_{j,x} + e_{(3,2)} u_{x,y} F_s N_{j,y} + e_{(3,3)} u_{x,z} F_{s,z} N_j\right) dV \\ \mathcal{E}\int_V \left(e_{(3,1)} u_{y,x} F_s N_{j,x} + e_{(3,2)} u_{y,y} F_s N_{j,y} + e_{(3,3)} u_{y,z} F_{s,z} N_j\right) dV \\ \mathcal{E}\int_V \left(e_{(3,1)} u_{z,x} F_s N_{j,x} + e_{(3,2)} u_{z,y} F_s N_{j,y} + e_{(3,3)} u_{z,z} F_{s,z} N_j\right) dV\end{Bmatrix} \tag{16}$$

The formulation of the vector is analogous to the thermal one. The resulting load vector is linearly related to the electric field, and no shear components arise under the present assumptions.

It is possible to collect these components in the governing equation written as:

$$\delta L_{int} = \delta\boldsymbol{q}_{sj}^T\left[\boldsymbol{K}_0^{ij\tau s} + \boldsymbol{K}_{lnl}^{ij\tau s} + \boldsymbol{K}_{nll}^{ij\tau s} + \boldsymbol{K}_{nlnl}^{ij\tau s}\right]\boldsymbol{q}_{\tau i} - \delta\boldsymbol{q}_{sj}^T\left[\boldsymbol{F}_{\theta_l}^{sj} + \boldsymbol{F}_{\theta_{nl}}^{sj}\right] - \delta\boldsymbol{q}_{sj}^T\left[\boldsymbol{F}_{p_l}^{sj} + \boldsymbol{F}_{p_{nl}}^{sj}\right] = 0 \tag{17}$$

In a compact form, the governing equation can also be rewritten as:

$$\delta\boldsymbol{q}_{sj}: \quad \boldsymbol{K}_s^{ij\tau s}\boldsymbol{q}_{\tau i} - \boldsymbol{F}_\theta^{sj} - \boldsymbol{F}_p^{sj} = 0 \tag{18}$$

Through the assembly procedure it is possible to rewrite Eq. (18) as follows:

$$\boldsymbol{K}_s\boldsymbol{q} - \boldsymbol{F}_\theta - \boldsymbol{F}_p = 0 \tag{19}$$

Eq. (19) describes a nonlinear set of equations that cannot be solved directly, and, as a consequence, it is necessary to introduce an incremental linearized scheme. In order to use the Newton-Raphson method [17], one can define the residual nodal force vector as:

$$\boldsymbol{\varphi}_{res} = \boldsymbol{K}_S\boldsymbol{q} - \boldsymbol{F}_\theta - \boldsymbol{F}_p \tag{20}$$

To solve the problem, it is necessary to minimize the residual nodal force vector since, at the equilibrium, the residual is null.

B. Newton-Raphson linearization scheme

It is possible to linearize the equation, expanding it in Taylor's series about the known solution $(\boldsymbol{q}, \Delta T)$. The piezoelectric contribution is kept constant during the analysis, since the actuators are considered to operate in an on/off mode. Eq. (20) is written as:

$$\boldsymbol{\varphi}_{res}(\boldsymbol{q} + \delta\boldsymbol{q}, \Delta\mathcal{T} + \delta\Delta\mathcal{T}) = \boldsymbol{\varphi}_{res}(\boldsymbol{q}, \Delta\mathcal{T}) + \left.\frac{\partial\boldsymbol{\varphi}_{res}}{\partial\boldsymbol{q}}\right|_{\boldsymbol{q}} \delta\boldsymbol{q} + \left.\frac{\partial\boldsymbol{\varphi}_{res}}{\partial(\Delta\mathcal{T})}\right|_{\Delta\mathcal{T}} \delta\lambda(\Delta\mathcal{T})_{ref} = 0 \tag{21}$$

In Eq. (21) it is assumed that the thermal load varies directly with the initial thermal loading $(\Delta\mathcal{T})_{ref}$ with a rate of change λ. It is possible to define a stiffness matrix called *tangent stiffness matrix* $\boldsymbol{K}_T = \left.\frac{\partial\boldsymbol{\varphi}_{res}}{\partial\boldsymbol{q}}\right|_{\boldsymbol{q}}$ and a new thermal load vector called *tangent thermal load vector* $\tilde{\boldsymbol{F}}_\theta = -\left.\frac{\partial\boldsymbol{\varphi}_{res}}{\partial(\Delta\mathcal{T})}\right|_{\Delta\mathcal{T}} (\Delta\mathcal{T})_{ref}$. Substituting the definitions of the matrix and the new vector, the Taylor expansion written in Eq. (21) becomes as follows.

$$\boldsymbol{\varphi}_{res}(\boldsymbol{q} + \delta\boldsymbol{q}, \Delta\mathcal{T} + \delta\Delta\mathcal{T}) = \boldsymbol{\varphi}_{res}(\boldsymbol{q}, \Delta\mathcal{T}) + \boldsymbol{K}_T\delta\boldsymbol{q} - \left(\tilde{\boldsymbol{F}}_{\theta_l} + \tilde{\boldsymbol{F}}_{\theta_{nl}}\right)\delta\lambda = 0 \tag{22}$$

$$\boldsymbol{K}_T\delta\boldsymbol{q} = \tilde{\boldsymbol{F}}_\theta\delta\lambda - \boldsymbol{\varphi}_{res}(\boldsymbol{q}, \Delta\mathcal{T}) \tag{23}$$

In these equations, the loading scaling parameter λ is introduced in the problem as a variable of the equation system. As a consequence, it is necessary to couple Eq. (23) with a general constraint equation to close the problem. The obtained system can be written as follows:

$$\begin{cases} \boldsymbol{K}_T\delta\boldsymbol{q} = \tilde{\boldsymbol{F}}_\theta\delta\lambda - \boldsymbol{\varphi}_{res} \\ \boldsymbol{c}(\delta\boldsymbol{q}, \delta\lambda) = 0 \end{cases} \tag{24}$$

The choice of the constraint equation defines the incremental scheme that will be followed in the numerical solution procedure. Depending on the constraint, it is possible to define, for instance, the load-control method with the relationship $\delta\lambda = 0$, the displacement-control method with $\delta\boldsymbol{q} = 0$ and the path following method acting on both $\delta\lambda$ and $\delta\boldsymbol{q}$. In the present work, the path-following method introduced by Crisfield [18] and later modified by Carrera [19] is adopted.

C. Derivation of the tangent stiffness matrix and tangent thermal vector

The tangent stiffness matrix is obtained by linearizing the virtual strain energy, as given by Eq. (25):

$$\delta^2 L_{int} = \delta\left(\int_V \delta\boldsymbol{\varepsilon}_m^T\boldsymbol{\sigma}dV\right) = \int_V \delta\boldsymbol{\varepsilon}_m^T\delta\boldsymbol{\sigma}dV + \int_V \delta^2\boldsymbol{\varepsilon}_m^T\boldsymbol{\sigma}dV \tag{25}$$

The first term of Eq. (25) demands the linearization of the constitutive Eqs. (7). It is assumed that the material properties do not depend on the unknown $\boldsymbol{q}$; as a consequence, the derivative operator acts on the strain part of the constitutive equations. After some manipulation, it is possible to obtain the first two terms of the tangent stiffness matrix that depend only on the mechanical component. In the first part of Eq. (25) the variational operator applied to the thermal and piezoelectric stress contributions gives null terms due to the definition of the thermal and piezoelectric stresses ($\boldsymbol{\sigma}_\theta = -\beta\Delta\mathcal{T}$, $\boldsymbol{\sigma}_p = -e\mathcal{E}$).

$$\begin{aligned} \int_V \delta\boldsymbol{\varepsilon}_m^T\delta\boldsymbol{\sigma}dV &= \int_V \delta(\boldsymbol{\varepsilon}_l + \boldsymbol{\varepsilon}_{nl})^T\delta(\boldsymbol{\sigma}_l + \boldsymbol{\sigma}_{nl})dV = \int_V \delta(\boldsymbol{\varepsilon}_l + \boldsymbol{\varepsilon}_{nl})^T\boldsymbol{C}\delta(\boldsymbol{\varepsilon}_l + \boldsymbol{\varepsilon}_{nl})dV \\ &= \int_V \delta\boldsymbol{\varepsilon}_l^T\boldsymbol{C}\delta\boldsymbol{\varepsilon}_l dV + \int_V \delta\boldsymbol{\varepsilon}_{nl}^T\boldsymbol{C}\delta\boldsymbol{\varepsilon}_l dV + \int_V \delta\boldsymbol{\varepsilon}_l^T\boldsymbol{C}\delta\boldsymbol{\varepsilon}_{nl} dV + \int_V \delta\boldsymbol{\varepsilon}_{nl}^T\boldsymbol{C}\delta\boldsymbol{\varepsilon}_{nl} dV \end{aligned} \tag{26}$$

Manipulating Eq. (26) it is possible to obtain Eq. (27) where the FNs of the tangent stiffness matrix are the same as those of the secant stiffness matrix. However, due to the variation of the nonlinear strain-displacement operator, the resulting tangent contribution is symmetric.

$$\int_V \delta\boldsymbol{\varepsilon}_m^T\delta\boldsymbol{\sigma}dV = \delta\boldsymbol{q}_{sj}^T\left[\boldsymbol{K}_0^{ij\tau s} + \boldsymbol{K}_{nll}^{ij\tau s} + 2\boldsymbol{K}_{lnl}^{ij\tau s} + 2\boldsymbol{K}_{nlnl}^{ij\tau s}\right]\delta\boldsymbol{q}_{\tau i} = \delta\boldsymbol{q}_{sj}^T\left[\boldsymbol{K}_0^{ij\tau s} + \boldsymbol{K}_{T1}^{ij\tau s}\right]\delta\boldsymbol{q}_{\tau i} \tag{27}$$

$\boldsymbol{K}_{T1}^{ij\tau s}$ is the nonlinear contribution of the tangent stiffness matrix. The second part of Eq. (25) is specified further in Eq. (28).

$$\int_V \delta^2\boldsymbol{\varepsilon}_m^T\boldsymbol{\sigma}dV = \int_V \delta^2\boldsymbol{\varepsilon}_l^T\boldsymbol{\sigma}dV + \int_V \delta^2\boldsymbol{\varepsilon}_{nl}^T\boldsymbol{\sigma}dV = \int_V \delta^2\boldsymbol{\varepsilon}_{nl}^T\boldsymbol{\sigma}dV \tag{28}$$

Eq. (28) can now be developed as follows:

$$\begin{aligned}
\int_V \delta^2\boldsymbol{\varepsilon}_{nl}^T\boldsymbol{\sigma}dV &= \int_V \left(\boldsymbol{B}_{nl}^* \begin{Bmatrix} \delta q_{x_{\tau i}}\delta q_{x_{sj}} \\ \delta q_{y_{\tau i}}\delta q_{y_{sj}} \\ \delta q_{z_{\tau i}}\delta q_{z_{sj}} \end{Bmatrix}\right)^T \boldsymbol{\sigma}dV = \int_V \left(\boldsymbol{B}_{nl}^* \begin{Bmatrix} \delta q_{x_{\tau i}}\delta q_{x_{sj}} \\ \delta q_{y_{\tau i}}\delta q_{y_{sj}} \\ \delta q_{z_{\tau i}}\delta q_{z_{sj}} \end{Bmatrix}\right)^T \left(\boldsymbol{\sigma}_l + \boldsymbol{\sigma}_{nl} + \boldsymbol{\sigma}_\theta + \boldsymbol{\sigma}_p\right) dV \\
&= \delta\boldsymbol{q}_{sj}^T \int_V diag\Big(\boldsymbol{B}_{nl}^{*T}(\boldsymbol{\sigma}_l + \boldsymbol{\sigma}_{nl} + \boldsymbol{\sigma}_\theta + \boldsymbol{\sigma}_p)\Big)dV\delta\boldsymbol{q}_{\tau i} \\
&= \delta\boldsymbol{q}_{sj}^T \left[\boldsymbol{K}_{\sigma l}^{ij\tau s} + \boldsymbol{K}_{\sigma nl}^{ij\tau s} + \boldsymbol{K}_{\sigma\theta}^{ij\tau s} + \boldsymbol{K}_{\sigma p}^{ij\tau s}\right]\delta\boldsymbol{q}_{\tau i} = \delta\boldsymbol{q}_{sj}^T \left[\boldsymbol{K}_{\sigma}^{ij\tau s} + \boldsymbol{K}_{\sigma\theta}^{ij\tau s} + \boldsymbol{K}_{\sigma p}^{ij\tau s}\right]\delta\boldsymbol{q}_{\tau i}
\end{aligned} \tag{29}$$

The first two matrices $\boldsymbol{K}_{\sigma l}$ and $\boldsymbol{K}_{\sigma nl}$ are the geometrical matrices which depend on mechanical stress and can be found in the literature [20]. The last two matrices collect the thermal and piezoelectric components and the explicit formulations are expressed by Eqs. (30) and (31).

$$\begin{aligned}
\boldsymbol{K}_{\sigma\theta}^{ij\tau s} = -\Delta\mathcal{T}\Big(&\beta_1 \int_h F_\tau F_s dz \int_\Omega N_{i,x}N_{j,x}dA + \beta_2 \int_h F_\tau F_s dz \int_\Omega N_{i,y}N_{j,y}dA + \beta_3 \int_h F_{\tau,z}F_{s,z}dz \int_\Omega N_i N_j dA + \\
&\beta_6 \int_h F_\tau F_s dz \int_\Omega N_{i,x}N_{j,y}dA + \beta_6 \int_h F_\tau F_s dz \int_\Omega N_{i,y}N_{j,x}dA\Big)\boldsymbol{I}
\end{aligned} \tag{30}$$

$$\boldsymbol{K}_{\sigma p}^{ij\tau s} = -\mathcal{E}\Big(e_{(3,1)} \int_h F_\tau F_s dz \int_\Omega N_{i,x}N_{j,x}dA + e_{(3,2)} \int_h F_\tau F_s dz \int_\Omega N_{i,y}N_{j,y}dA + e_{(3,3)} \int_h F_{\tau,z}F_{s,z}dz \int_\Omega N_i N_j dA\Big)\boldsymbol{I} \tag{31}$$

Where $\boldsymbol{I}$ denotes the 3×3 identity matrix, $dA = dxdy$, Ω is the reference surface and h is the thickness.

The summation of the components given by Eq. (27) and Eq. (29) allows obtaining the FNs of the complete tangent stiffness matrix as follows:

$$\begin{aligned}
\delta\boldsymbol{q}_{sj}^T\boldsymbol{K}_T^{ij\tau s}\delta\boldsymbol{q}_{\tau i} &= \int_V \delta\boldsymbol{\varepsilon}_m^T\delta\boldsymbol{\sigma}dV + \int_V \delta^2\boldsymbol{\varepsilon}_m^T\boldsymbol{\sigma}dV \\
&= \delta\boldsymbol{q}_{sj}^T\left[\boldsymbol{K}_0^{ij\tau s} + \boldsymbol{K}_{T1}^{ij\tau s}\right]\delta\boldsymbol{q}_{\tau i} + \delta\boldsymbol{q}_{sj}^T\left[\boldsymbol{K}_{\sigma l}^{ij\tau s} + \boldsymbol{K}_{\sigma nl}^{ij\tau s} + \boldsymbol{K}_{\sigma\theta}^{ij\tau s} + \boldsymbol{K}_{\sigma p}^{ij\tau s}\right]\delta\boldsymbol{q}_{\tau i} \\
&= \delta\boldsymbol{q}_{sj}^T\left[\boldsymbol{K}_0^{ij\tau s} + \boldsymbol{K}_{T1}^{ij\tau s} + \boldsymbol{K}_{\sigma l}^{ij\tau s} + \boldsymbol{K}_{\sigma nl}^{ij\tau s} + \boldsymbol{K}_{\sigma\theta}^{ij\tau s} + \boldsymbol{K}_{\sigma p}^{ij\tau s}\right]\delta\boldsymbol{q}_{\tau i}
\end{aligned} \tag{32}$$

Writing the governing equation in Taylor's series as given by Eq. (21) allows finding a new vector defined as $\tilde{\boldsymbol{F}}_\theta = -\left.\frac{\partial\boldsymbol{\varphi}_{res}}{\partial(\Delta\mathcal{T})}\right|_{\Delta\mathcal{T}} (\Delta\mathcal{T})_{ref}$. Applying this definition in Eq. (33), it is possible to write the FN of this vector.

$$\tilde{\boldsymbol{F}}_\theta = -\left.\frac{\partial(\boldsymbol{K}_s\boldsymbol{q} - \boldsymbol{F}_\theta - \boldsymbol{F}_p)}{\partial\Delta\mathcal{T}}\right|_{\Delta\mathcal{T}} (\Delta\mathcal{T})_{ref} = \left.\frac{\partial(\boldsymbol{F}_\theta)}{\partial\Delta\mathcal{T}}\right|_{\Delta\mathcal{T}} (\Delta\mathcal{T})_{ref} \tag{33}$$

The tangent vector nuclei are given by Eqs. (34) and (35).

$$\tilde{\boldsymbol{F}}_{\theta_l}^{sj} = (\Delta\mathcal{T})_{ref}\cdot \begin{Bmatrix} \int_V \left[\beta_1 F_s N_{j,x} + \beta_6 F_s N_{j,y}\right] dV \\ \int_V \left[\beta_2 F_s N_{j,y} + \beta_6 F_s N_{j,x}\right] dV \\ \int_V \beta_3 F_{s,z} N_j dV \end{Bmatrix} \tag{34}$$

$$\tilde{\boldsymbol{F}}^{sj}_{\theta_{nl}} = (\Delta\mathcal{T})_{ref}\cdot\begin{Bmatrix}\int_V \left[\beta_1 u_{x,x}F_sN_{j,x} + \beta_2 u_{x,y}F_sN_{j,y} + \beta_3 u_{x,z}F_{s,z}N_j + \beta_6\left(u_{x,x}F_sN_{j,y} + u_{x,y}F_sN_{j,x}\right)\right] dV \\ \int_V \left[\beta_1 u_{y,x}F_sN_{j,x} + \beta_2 u_{y,y}F_sN_{j,y} + \beta_3 u_{y,z}F_{s,z}N_j + \beta_6\left(u_{y,x}F_sN_{j,y} + u_{y,y}F_sN_{j,x}\right)\right] dV \\ \int_V \left[\beta_1 u_{z,x}F_sN_{j,x} + \beta_2 u_{z,y}F_sN_{j,y} + \beta_3 u_{z,z}F_{s,z}N_j + \beta_6\left(u_{z,x}F_sN_{j,y} + u_{z,y}F_sN_{j,x}\right)\right] dV\end{Bmatrix} \quad (35)$$

It is important to consider this additional term in the description of the nonlinear thermal problem. The nonlinear component expressed by Eq. (35) is dependent on the displacement value. Therefore, a path-following constraint, which simultaneously controls the load and displacement parameters, is advisable for a good convergence trend.

IV. Numerical results

A first analysis is conducted on a straight-fiber laminated plate with piezoelectric actuators applied as external layers of the stacking sequence. The present results are compared with the displacement response reported in [10]. The lamination is $(P/(0/90)_2)_s$ where P denotes the piezoelectric patch. The patch is made of PZT-5A, which is modeled as an isotropic material with the following properties: $E = 63.0$ GPa, $G = 24.2$ GPa, $\nu = 0.3$, $\alpha = 0.9\times10^{-6}/°C$ and $d_{31} = d_{32} = 2.54\times10^{-10}$ m/V. The plate is composed of Graphite/epoxy orthotropic layers whose properties are: $E_{11} = 150.0$ GPa, $E_{22} = E_{33} = 9.0$ GPa, $G_{12} = G_{13} = 7.1$ GPa, $G_{23} = 2.5$ GPa, $\nu_{12} = 0.3$, $\alpha_{11} = 1.1\times10^{-6}/°C$, $\alpha_{22} = \alpha_{33} = 25.2\times10^{-6}/°C$.

The plate is square-shaped with a thickness of $t = 1.2$ mm and a ratio edge/thickness equal to $L/t = 100$, whereas the piezo layers are 0.1 mm thick each. The temperature distribution is assumed to be uniform across the plate, and three different voltage values are applied to the patch to evaluate their influence on the buckling critical temperature and post-buckling shapes. The voltages are the same for the upper and lower patches, being $\Delta V = 100$ V, $\Delta V = 0$ V, $\Delta V = -100$ V with a consequent electric field of $E = 1.0\times10^6$ V/m , $E = 0$ V/m , $E = -1.0\times10^6$ V/m . The zero-voltage case is considered as a reference configuration to assess the effect of actuator activation. The edges are simply supported, where the constraints are applied on the middle line of the plate: the z displacement is imposed to zero at each edge, and the edges are fixed against normal displacements and allowed to translate in the tangential direction.

A first convergence analysis is conducted, and 21×21 Q9 elements are chosen with LE2 expansion theory, one for each layer. Table 1 reports the linearised critical temperature for the three different piezoelectric activations. The same configurations are analysed through a nonlinear analysis, and the central displacement is reported in Fig. 1. The findings indicate that the applied voltage has a substantial impact on the thermal buckling response. Applying a

Table 1 Linearised critical buckling temperature, 21×21 **Q9 elements are chosen with LE2 expansion theory.**

	$\Delta V = 100V$	$\Delta V = 0$	$\Delta V = -100V$
$\Delta T_{cr}\,[°C]$	29.15	46.5	65.2

positive voltage anticipates buckling, while a negative voltage raises the critical temperature and consequently delays the onset of instability. Figure 1 shows a very good agreement between the present CUF–FEM results and the reference solution [10] for all the considered actuation levels. The activation of the piezoelectric layers can either decrease or increase the critical buckling temperature, thereby advancing or delaying the onset of thermal buckling. Figure 2 reports the central stress distribution for the different configurations at a fixed temperature of $\Delta T = 75.5°C$. As shown in the equilibrium path, this temperature corresponds to different values of displacement. The through-thickness stress distributions reported in Fig. 2 show that σ_{xx} and σ_{yy} follow similar trends for the three actuation levels, while their magnitude is significantly affected by the applied voltage. Significant stress gradients occur near the interfaces between the piezoelectric layers and the composite laminate, confirming the need for refined through-the-thickness kinematics. The effect of the piezoelectric actuation is particularly evident in the transverse normal stress σ_{zz}, whose distribution changes with the applied voltage. This behavior is associated with the actuation mechanism and with the mismatch between the piezoelectric and composite layers.

V. Conclusion

A higher-order CUF–FEM formulation has been presented for the geometrically nonlinear thermo-piezo-mechanical analysis of laminated composite plates with piezoelectric actuators. Thermal and piezoelectric effects are modeled

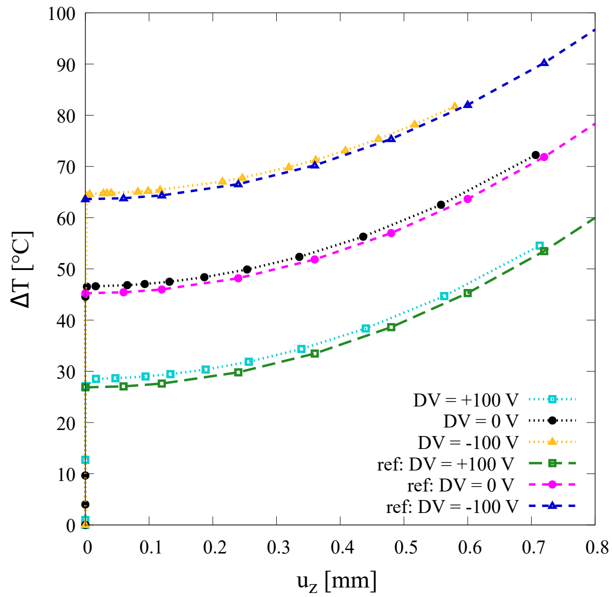

Fig. 1 Present method compared to the reference results [10]. Analysis conducted with 21×21 Q9 elements with LE2 expansion theory.

through a decoupled approach, and the kinematics of the problem are expressed with higher-order theories. The nonlinear problem is solved using the Newton Raphson iterative procedure combined with the arc-length constraint.

The numerical results demonstrate the accuracy of the proposed approach by comparison with reference post-buckling results. The activation of the piezoelectric layers is shown to significantly affect the critical buckling temperature and the nonlinear equilibrium path. Depending on the applied voltage, the onset of buckling can be either anticipated or delayed. Moreover, the stress distributions highlight relevant through-thickness variations, especially near the piezoelectric/composite interfaces.

The proposed framework therefore represents an effective tool for the analysis and design of smart composite structures subjected to combined thermal and piezoelectric actuation.

References

[1] Reddy, J., "On laminated composite plates with integrated sensors and actuators," *Engineering Structures*, Vol. 21, No. 7, 1999, pp. 568–593. https://doi.org/10.1016/s0141-0296(97)00212-5.

[2] Riks, E., "Buckling," , Dec. 2017. https://doi.org/10.1002/9781119176817.ecm2027.

[3] Gossard, M., Seide, P., and Roberts, W., "Thermal buckling of plates," Tech. rep., 1952.

[4] Guo, W., Li, Y., Li, Y., Tian, S., and Wang, S., "Thermal–structural analysis of large deployable space antenna under extreme heat loads," *Journal of Thermal Stresses*, Vol. 39, No. 8, 2016, pp. 887–905. https://doi.org/10.1080/01495739.2016.1189776.

[5] Appel, S., *Simulation of thermoelastic behaviour of spacecraft structures*, Springer aerospace technology, Springer, Cham, 2022. Literaturangaben.

[6] Kuriakose, V., and Sreehari, V., "Vibration and flutter analysis of damaged composite plates under thermal environment and its passive control using piezoelectric patches," *Composites Part C: Open Access*, Vol. 11, 2023, p. 100361. https://doi.org/10.1016/j.jcomc.2023.100361.

[7] Yazdani, S., Kiani, Y., Jabbari, M., and Eslami, M. R., "Thermal Buckling of Piezoelectric Composite Beam," *ISRN Mechanical Engineering*, Vol. 2011, 2011, pp. 1–11. https://doi.org/10.5402/2011/362030.

[8] Zhang, Y., Xue, Y., Yuan, W., Ma, W., Li, J., and Li, F., "Active Control of Thermo-mechanical Buckling of Composite Laminated Plates Using Piezoelectric Actuators," *Acta Mechanica Solida Sinica*, Vol. 34, No. 3, 2021, pp. 369–380. https://doi.org/10.1007/s10338-020-00209-5.

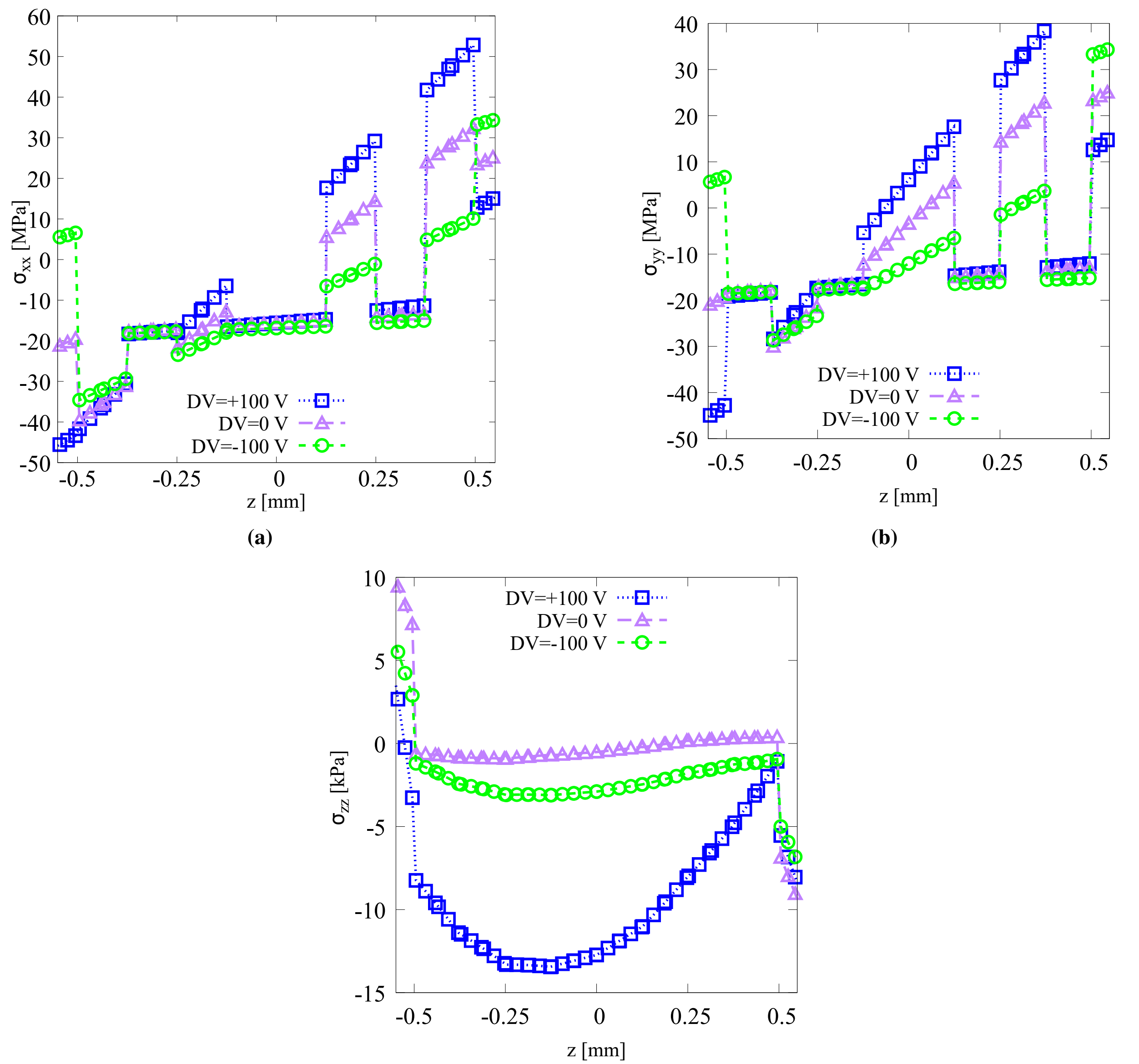

(a) **(b)**

(c)

Fig. 2 Stress distribution along the thickness for $\Delta T = 75.5°C$. Analyses made with 21×21 Q9 and LE2 expansion function.

[9] Mirzavand, B., and Bohlooly, M., "Thermal Buckling of Piezolaminated Plates Subjected to Different Loading Conditions," *Journal of Thermal Stresses*, Vol. 38, No. 10, 2015, pp. 1138–1162. https://doi.org/10.1080/01495739.2015.1073506.

[10] Shen, H., "Thermal postbuckling of shear-deformable laminated plates with piezoelectric actuators," *Composites Science and Technology*, Vol. 61, No. 13, 2001, pp. 1931–1943. https://doi.org/10.1016/s0266-3538(01)00099-9.

[11] OH, I., HAN, J., and LEE, I., "Postbuckling and vibration characteristics of piezolaminated composite plate subject to thermo-piezoelectric loads," *Journal of Sound and Vibration*, Vol. 233, No. 1, 2000, pp. 19–40. https://doi.org/10.1006/jsvi.1999.2788.

[12] Nagai, T., M.and Ikeda, and Miyazaki, N., "Stress intensity factor analysis of a three-dimensional interface crack between dissimilar anisotropic materials under thermal stress," *Engineering Fracture Mechanics*, Vol. 91, 2012, pp. 14–36. https://doi.org/10.1016/j.engfracmech.2012.04.017.

[13] Rao, S. S., *The finite element method in engineering*, 5th ed., Elsevier/Butterworth Heinemann, Amsterdam, 2011.

[14] Washizu, K., *Variational Methods in Elasticity and Plasticity*, Pergamon, Oxford, 1968.

[15] Pagani, A., Bracaglia, F., Zappino, E., and Carrera, E., “Nonlinear thermal stresses analysis and post-buckling of rectangular composite laminates using high-order plate finite elements,” *Journal of Thermal Stresses*, 2026. https://doi.org/10.1080/01495739.2026.2676322.

[16] Carrera, E., Zappino, E., Cinefra, M., and Petrolo, M., *Finite element analysis of structures through unified formulation*, Wiley, Chichester, West Sussex, 2014.

[17] Reddy, J. N., *An introduction to nonlinear finite element analysis*, second edition, first published in paperback ed., Oxford University, Oxford, 2020.

[18] Crisfield, M., “An arc-length method including line searches and accelerations,” *International Journal for Numerical Methods in Engineering*, Vol. 19, No. 9, 1983, pp. 1269–1289. https://doi.org/10.1002/nme.1620190902.

[19] Carrera, E., “A study on arc-length-type methods and their operation failures illustrated by a simple model,” *Computers & Structures*, Vol. 50, No. 2, 1994, pp. 217–229. https://doi.org/10.1016/0045-7949(94)90297-6.

[20] Wu, B., Pagani, A., Filippi, M., Chen, W., and Carrera, E., “Large-deflection and post-buckling analyses of isotropic rectangular plates by Carrera Unified Formulation,” *International Journal of Non-Linear Mechanics*, Vol. 116, 2019, pp. 18–31. https://doi.org/10.1016/j.ijnonlinmec.2019.05.004.